

MD and OKMC simulations of the displacement cascades in nickel

Wen-Jing Xiao¹ · Gui-Yan Wu¹ · Mei-Heng Li¹ · Hui-Qiu Deng¹ · Wei Zhang² · Ping Huai² · Wang-Yu Hu¹

Received: 17 May 2015 / Revised: 20 July 2015 / Accepted: 11 August 2015 / Published online: 9 May 2016
© Shanghai Institute of Applied Physics, Chinese Academy of Sciences, Chinese Nuclear Society, Science Press China and Springer Science+Business Media Singapore 2016

Abstract The molecular dynamics (MD) method was used to investigate the displacement cascades with primary knock-on atom (PKA) energies of 2–40 keV at 100 and 600 K. The migration energy of defects and their clusters was calculated by nudged elastic band (NEB) method. Object kinetic Monte Carlo (OKMC) was used to simulate the evolution of defects in Ni under annealing. In each annealing stage, the recombination mechanism was discussed and evolution of the defects under different cascade conditions was compared. It was found that the defects generated in high-temperature cascades are more stable than those in the low-temperature cascades. In addition, almost all the defects are annihilated during annealing process at low PKA energy. At PKA energy of 20–40 keV, however, a large number of defects would remain after annealing.

Keywords Displacement cascades · Molecular dynamics simulation · Object kinetic Monte Carlo

This study was supported by the CAS Strategically Leading Program of the Chinese Academy of Sciences (XD02004140) and the National Natural Science Foundation of China (Nos. 51371080, 11076012).

✉ Wang-Yu Hu
wyuhu@hnu.edu.cn

¹ Department of Applied Physics, School of Physics and Electronics, Hunan University, Changsha 410012, China

² Shanghai Institute of Applied Physics, Chinese Academy of Sciences, Shanghai 201800, China

1 Introduction

Thorium molten salt reactor (TMSR) is considered as a candidate of the generation 4 reactors [1, 2]. Due to the excellent high-temperature properties and corrosion resistance, Hastelloys are important structural materials for advanced nuclear reactors [3, 4]. Ni is the major element in Hastelloys, and its irradiation property has been discussed for decades. By comparing the displacement cascades in Cu and Fe with Ni, King et al. [5] and Kwon et al. [6] found that more residual defects could be generated and more point defects were able to get clustered in Cu and Fe than those in Ni. Several interatomic potentials for Ni were used to investigate the effect of stacking fault energy (SFE) on cascade evolution [7]. The results showed that it was easier for the stacking fault tetrahedron (SFT) to form at lower SFE.

Additionally, the spatial and timescales accessible to molecular dynamics (MD) simulation are only nanometers and nanoseconds. Therefore, MD simulation is limited for the practical prediction of microstructural evolution for long timescale. A solution to solve this problem is the application of the object kinetic Monte Carlo (OKMC) method together with MD, which has been successfully proved in defect simulations in Fe and Cu annealing [8–10], by simulating the damage using the MD method. Based on the cascade simulations, Almazouzi [11] used the KMC method to describe the long-term evolution of the defects in Ni and showed that the annealing temperature affected the fraction of the defects that escaped the KMC boundary strongly. Only the diffusion of monovacancy and divacancy was considered in the study, and low primary knock-on atom (PKA) energy ($E_P < 10$ keV) cascades were simulated. It was found that almost 90 % of the MD-produced defects might be freely migrating defects at

annealing temperatures of >500 K. However, the study did not consider the migration of big vacancy clusters, the influences of irradiation at high temperatures, and PKA energies on the evolution of the defects in Ni.

Large clusters will form in the cascades under high energy at high temperature. So, it is necessary to consider the migrations for more types of defects. In this paper, we simulate the cascades in Ni at high energy and temperature. The nudged elastic band (NEB) method is used to simulate the migration energies for more kinds of defects. The evolutions of defects are studied by the OKMC method. These methods can accurately describe the long-term evolution of the defects produced by a displacement cascade, and we can be prepared for studying Hastelloy alloy in the future.

2 Simulation methods

In this paper, a modified analytic embedded-atom method (MAEAM) potential, which has been successfully applied to metallic systems, is used to do MD simulations. The energy of every atom (E_i) in a crystal is given by

$$E_i = \frac{1}{2} \sum_{j \neq i} \varphi(r_{ij}) + F(\rho_i) + M(P_i), \quad (1)$$

where $\Phi(r_{ij})$ is the pairwise interaction between atoms i and j with a pair separation of r_{ij} ; $M(P_i)$ is the exponential modification item; and $F(\rho_i)$ is the embedding energy. The potential functions are described in detail by Wang et al. [12]. The potential parameters for Ni are given in Table 1.

In this paper, we use a modified MOLDY code to study the displacement cascades in Ni. All simulation blocks in a size of $60a_0 \times 60a_0 \times 60a_0$ (864,000 atoms) are firstly equilibrated at 100 and 600 K for about 10 ps in NVT ensemble, where a_0 is the lattice constant of Ni. Then, a primary knock-on atom of $E_p = 2\text{--}40$ keV is initialized in a block center. Five different directions are assigned to the PKA to get the statistical results. The cascade simulation time with MD is 10 ps under each radiation condition, so that the cascade region can be cooled down completely. The Wigner–Seitz cell method is utilized to identify the

defects [13]. The distribution of defects obtained from the MD simulations is used as the input data for OKMC simulations [14].

Other input parameters for OKMC simulations are the migration energies of various defects in Ni. The NEB method is used to calculate the migration barriers [15, 16], which is easier and more reliable than the MD method in calculating the migration energies. The binding energies of different defects are calculated by the MD method. All the energies are calculated in the box of $10a_0 \times 10a_0 \times 10a_0$. In order to find the most stable structure of defect clusters, all possible configurations of the defects of the same size are considered. A defect of the lowest formation energy and the biggest binding energy is the most stable structure.

Based on the above results, the OKMC is mainly used to simulate the evolution of radiation-induced defects. The defects can be translated randomly or in accordance with the special direction in the crystal lattice. As used widely in radiation damage simulations, only the positions of transition objects are considered [17, 18]. The objects which can be treated with OKMC codes include vacancies, self-interstitial atoms (SIAs), and their clusters. In this model, defects are assumed to be spherical and their specific atomic structures are ignored. Four types of events can be considered in these objects: (1) jump to a neighbor position; (2) recombination between anti-type defects or coarsening between non-anti-type defects; (3) emission of an element from a defect cluster; and (4) annihilation and sink of mobile defects at grain boundaries, free surfaces, or dislocations. The pre-factors of diffusion in annealing simulations are taken from Ref [19]. The box size of OKMC simulations is $(105 \text{ nm})^3$, and periodic boundary conditions (PBC) are used in the simulations. Residual defects in the cascade collisions are annealed at 30–800 K, and each simulation is repeated 20 times to ensure good statistics.

3 Results and discussion

3.1 Validation of potential

The potential was tested, and the defect formation energies of single vacancy (E_{vac}), dumbbells in different directions ($E_{\text{d-111}}$, $E_{\text{d-110}}$, and $E_{\text{d-100}}$), SIA initialized in octahedral or tetrahedral interstitial site (E_{oct} and E_{tet}), and the elastic constants (C_{11} , C_{12} , and C_{44}) were calculated, as shown in Table 2, together with the results of other authors. It can be seen that the stability order of the defects is $E_{\text{d-100}} < E_{\text{d-110}} < E_{\text{d-111}} < E_{\text{oct}} < E_{\text{tet}}$ and the dumbbell in $\langle 100 \rangle$ direction has the lowest formation energy. Our results are closely related to the following studies on defects migration. The formation energies of different

Table 1 Optimized parameter values of MAEAM potential for Ni

F_0	2.9545685	k_c	0.05
n	0.355	k_0	$-2.1557471\text{e}+02$
ρ_e	12.976133	k_1	1.3880198
P_e	12.714634	k_2	-1.0619366
α	$-1.6501104\text{e}-3$	k_3	$-9.6388310\text{e}-01$
β	4.69	u_1	1.0
γ	5.41	u_2	1.5

Table 2 Defect formation energies and elastic constants for Ni

Authors	Defect formation energies (eV)						Elastic constant (GPa)		
	E_{vac}	E_{d-111}	E_{d-110}	E_{d-100}	E_{oct}	E_{tet}	C_{11}	C_{12}	C_{44}
This work	1.51	4.84	4.62	4.00	5.23	6.10	260.7	150.7	126.0
MD [20]	1.95	5.31	–	5.26	5.28	6.64	257	155	136
DFT [21]	1.5–1.7	4.24	–	4.08	–	–	261.2	150.8	131.7
Exp. [22]	1.63	–	–	–	–	–	260	150	126

kinds of defects and elastic constants agree well with those from previous simulations [20, 21] and experimental results [22].

3.2 Defect production in Ni

Figure 1 shows the mean number of SIA–vacancy pairs (N_F) value for the cascades of Ni in this work and other metals in Ref. [23] at 100 K (initial temperature) at different PKA energies (E_p) and the N_F – E_p curve at 600 K obtained in this work. The N_F increases with E_p . Only a few defects survive at $E_p < 10$ keV. The number of defects is over 100 at $E_p > 40$ keV. As atoms of high energy collide intensively, more defects are formed in the box. The defect production curve N_F in log–log scales fits excellently the Bacon power law of $N_F = AE_p^m$, where $A = 4.20$ and $m = 0.91$ at 100 K in Ni, though they depend weakly on material and temperature. At 600 K (Fig. 1b), we have $N_F = 2.82E_p^{1.02}$.

Figure 2 shows the distributions of defects in stable state at 600 K with $E_p = 2$ and 40 keV. The box size was diminished six times in Fig. 2a in order to observe the defect distribution clearly. At 2 keV, only a few individual defects remained in the box, while at 40 keV, the defects

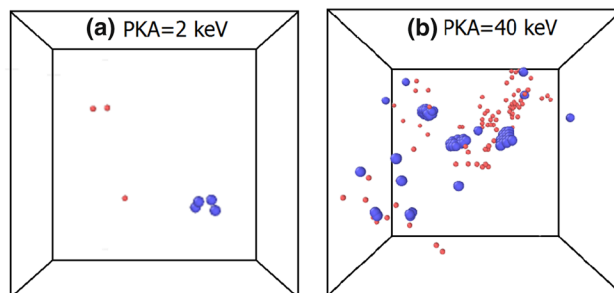


Fig. 2 Vacancies (red dots) and self-interstitial atoms (blue dots) generated in cascade collision at 600 K and $E_p = 2$ and 40 keV. (Color figure online)

number reached one hundred. In this condition, clusters of self-interstitial atoms distribute at the center of collision region, surrounded by vacancies without the formation of stacking fault tetrahedral (SFT) structure.

3.3 Defect energetics

The migration energies of various defects are listed in Table 3. In this paper, a single defect (interstitial and vacancy) has a three-dimensional migration regime. The I_2 and I_3 (I_n means the cluster consists of n interstitial atoms) clusters have similar ground-state configurations of the $\langle 100 \rangle$ dumbbell. Larger defect clusters migrate via the one-dimensional mechanism without direction change. The dumbbells in the configuration of I_4 are not aligned and not discussed here. The vacancies are assumed as immobile with the cluster size of >4 . Similar results were reported in

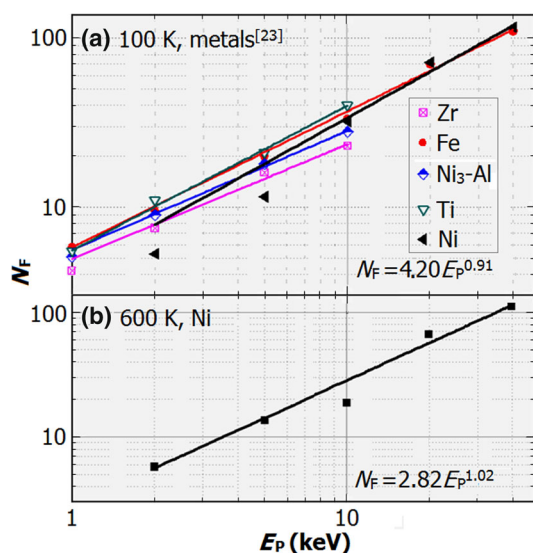


Fig. 1 Log–log plots of N_F vs E_p at initial temperatures of **a** 100 K and **b** 600 K

Table 3 Migration energies (E_m , in eV) of interstitials (I) and vacancies (V) in Ni

Defect types	This work	MD simulated [11]	Measured
V_1	1.395	0.85	1.1/1.8 [24]
V_2	1.478	0.57	0.83 [25]
V_3	1.529	–	–
V_4	1.501	–	–
I_1	0.250	0.12	0.14–0.18 [26]
I_2	0.103	0.1	0.12 [27]
I_3	0.326	0.1	–

Ref. [9]. Using the NEB method can simulate more types of the migration energies than MD method. The migration energies we obtained are compared with the experimental value. The migration energies of the single defect (V_1 and I_1) simulated by MD [11] are slightly lower than the experimental value.

It is believed that clusters are mobile, but the mobility decreases as defect size increases. The migration energies of SIA and SIA clusters are much lower than those of vacancy clusters, which leads to different behaviors during the evolution of defects. The binding energies of vacancies and interstitials in a cluster of size (n) are given by:

$$E_{b-v} = 0.35n^{0.26}, \quad (2)$$

$$E_{b-I} = 0.27n^{2.19}. \quad (3)$$

3.4 Annealing simulations

Based on the results of MD simulations and NEB calculations, the evolution of defects in bulk Ni was studied with OKMC simulations. Figure 3a shows the evolution of defects in bulk Ni after displacement cascades at 100 K and 40 keV. The annealing process has three stages. Stage I corresponding to the correlated recombinations is observed at 112 K, mainly resulted from the recombination of the single interstitials and vacancies. In the simulations in Ref. [11], the Stage I temperature was 57 K and was lower than the experimental value. At about 145 K, the clusters began to annihilate.

Stage II begins at 338 K. This stage mainly due to recombination of the defect clusters. The temperature of Stage II agrees with the experimental value of 350 K. Stage III is attributed to the dissociation of defect clusters at about 535 K. After the annealing process, 61 % defects are residual and all in the form of cluster.

Figure 3b shows the simulated evolution process for defects produced in the cascades at 600 K and 40 keV. Most defects are annihilated at Stage I, which is similar to the Stage I at 100 K. But in Stage II, recombination of the defect clusters at 600 K is significantly less than those at 100 K. And in Stage III the defect number keeps almost the same. This reason is that the defect clusters formed at the high-temperature cascade are more stable than at the low-temperature cascade. So that the defect clusters at the high-temperature cascade are difficult to emit defects during the annealing process. After the annealing process, 69 % defects remained in the box.

Figure 4 shows the number of surviving defects during annealing, for $E_p = 2-40$ keV at irradiation temperature of 600 K. It can be seen that Stage I temperature for $E_p = 2$ keV is obvious lower than those of the higher PKA energies. This is mainly due to different configurations of the defects. As shown in Fig. 2a, the defects at $E_p = 2$ keV are just individual defects, which are easier to migrate than clustered defects. For $E_p = 2$ keV, there was only one recombination stage in the annealing process, and all the defects were annihilated at last. At $E_p = 10$ keV, three stages appeared in the annealing process and no defects remained after annealing. At $E_p = 20$ keV, a modest increase of defect appeared, at annealing temperature of 550 K. This is due to the new emission of defect in the annealing process. Previous analysis showed that under high PKA energy and irradiation conditions, defect clusters of large sizes could be generated. This kind of clustered defect can emit single defect to reduce its size. However, the increase in size of the point defect cluster will increase the binding energy and decrease the emission probability of the cluster. These defect clusters are difficult to annihilate. At $E_p = 20$ and 40 keV, there are still a large number of defects (58 and 69 %) at annealing temperature of 800 K.

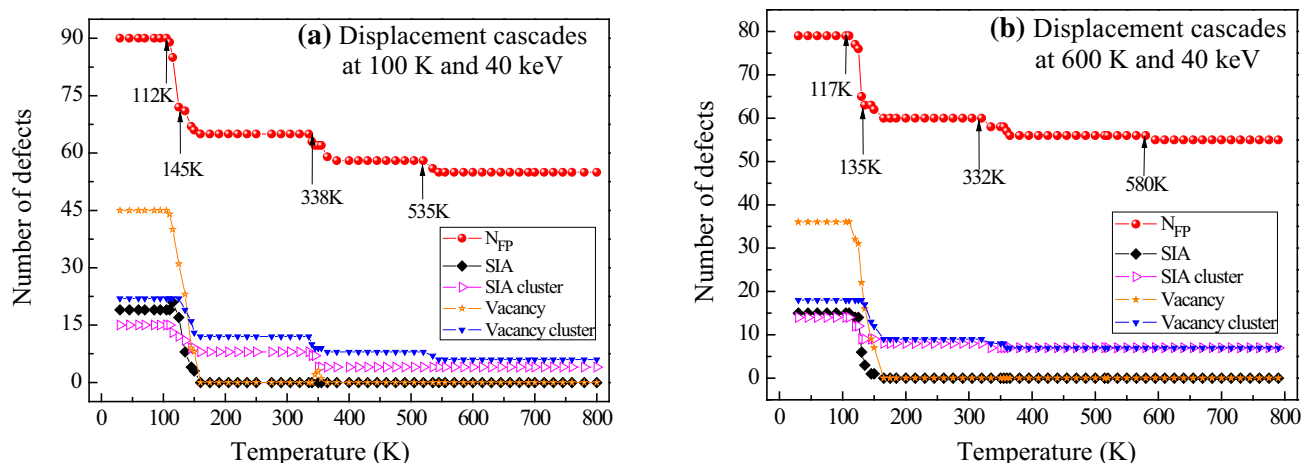


Fig. 3 Simulated number of surviving defects in annealing of bulk Ni after displacement cascades at 40 keV at 100 and 600 K

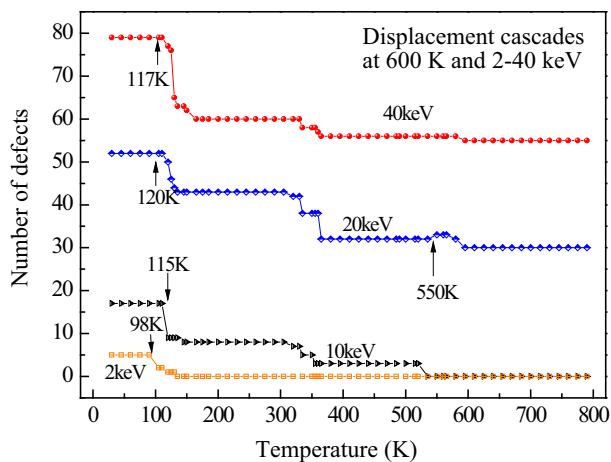


Fig. 4 Simulated number of surviving defects in annealing of bulk Ni after displacement cascades at 600 K and $E_p = 2\text{--}40$ keV

4 Conclusion

The MD method was used to investigate the displacement cascades, and the $N_F\text{--}E_p$ curve shows log–log scales. The migration energies calculated by NEB method agree well with experimental value.

OKMC was used to simulate the evolutions of defects in Ni under different irradiation conditions. The evolution stages are as follows: Stage I at about 115 K, Stage II at about 350 K, and Stage III at about 550 K.

The defects generated in high-temperature cascades are more stable than those in the low-temperature cascades. At $E_p \leq 10$ keV, almost all the defects annihilate in the annealing process, while at $E_p \geq 20$ keV, about 60 % of the defects remain after annealing process.

References

1. L. Zhu, P. Pu, S. Du et al., Simulation of neutron diffusion and transient analysis of MSR. *Nucl. Sci. Tech.* **25**, 020601 (2014). doi:[10.13538/j.1001-8042/nst.25.020601](https://doi.org/10.13538/j.1001-8042/nst.25.020601)
2. X. Zhou, G. Liu, Study of control rod worth in the TMSR. *Nucl. Sci. Tech.* **24**, 010601 (2013). doi:[10.13538/j.1001-8042/nst.2013.01.003](https://doi.org/10.13538/j.1001-8042/nst.2013.01.003)
3. J.R. Keiser, *Compatibility studies of potential molten-salt breeder reactor materials in molten fluoride salts* (Oak Ridge National Laboratory, Tennessee, 1977)
4. W.G. Liu, H. Han, C.L. Ren et al., The effect of Nb additive on Te-induced stress corrosion cracking in Ni alloy: a first-principles calculation. *Nucl. Sci. Tech.* **25**(5), 050603 (2014). doi:[10.13538/j.1001-8042/nst.25.050603](https://doi.org/10.13538/j.1001-8042/nst.25.050603)
5. W.E. King, R. Benedek, Computer simulation study of the displacement threshold-energy surface in Cu. *Phys. Rev. B* **23**, 6335–6339 (1981). doi:[10.1103/PhysRevB.23.6335](https://doi.org/10.1103/PhysRevB.23.6335)
6. J. Kwon, W. Kim, J.H. Hong, Comparison of the primary damage states in iron and nickel by molecular dynamics simulations. *Radiat. Eff. Defect. S* **4**, 207–218 (2006). doi:[10.1080/10420150600704013](https://doi.org/10.1080/10420150600704013)
7. Z. Yao, M.J. Caturla, R. Schaublin, Study of cascades damage in Ni by MD with different interatomic potentials. *J. Nucl. Mater.* **367**, 298–304 (2007). doi:[10.1016/j.jnucmat.2007.03.136](https://doi.org/10.1016/j.jnucmat.2007.03.136)
8. M.J. Caturla, N. Soneda, T. Diaz de la Rubia et al., Kinetic Monte Carlo simulations applied to irradiated materials: the effect of cascade damage in defect nucleation and growth. *J. Nucl. Mater.* **351**, 78–87 (2006). doi:[10.1016/j.jnucmat.2006.02.019](https://doi.org/10.1016/j.jnucmat.2006.02.019)
9. C.C. Fu, J.D. Torre, F. Willaime et al., Multiscale modelling of defect kinetics in irradiated iron. *Nat. Mater.* **4**, 68–74 (2005). doi:[10.1038/nmat1286](https://doi.org/10.1038/nmat1286)
10. F. Gao, D.J. Bacon, A.V. Barashev et al., Kinetic Monte Carlo annealing simulation of damage produced by cascades in alpha-iron. *Mater. Res. Soc. Symp. Proc.* **540**, 703–710 (1999)
11. A. Almazouzi, M.J. Caturla, T. Diaz de la Rubia et al., Annealing kinetics of single displacement cascades in Ni: an atomic scale computer simulation. *Mater. Res. Soc. Symp. Proc.* **540**, 685–690 (1999). doi:[10.1557/PROC-540-685](https://doi.org/10.1557/PROC-540-685)
12. K. Wang, S.F. Xiao, H.Q. Deng et al., An atomic study on the shock-induced plasticity and phase transition for iron-based single crystals. *Int. J. Plast.* **59**, 180–198 (2014). doi:[10.1016/j.ijplas.2014.03.007](https://doi.org/10.1016/j.ijplas.2014.03.007)
13. W.R. Bowen, F. Jenner, Dynamic ultrafiltration model for charged colloidal dispersions: a Wigner-Seitz cell approach. *Chem Eng Sci* **50**, 1707–1736 (1995). doi:[10.1016/0009-2509\(95\)00026-2](https://doi.org/10.1016/0009-2509(95)00026-2)
14. C. Domain, C.S. Becquart, L. Malerba, Simulation of radiation damage in Fe alloys: an object kinetic Monte Carlo approach. *J. Nucl. Mater.* **335**, 121–145 (2004). doi:[10.1016/j.jnucmat.2004.07.037](https://doi.org/10.1016/j.jnucmat.2004.07.037)
15. G.K. Schenter, G. Mills, H. Jonsson, Reversible work based quantum transition state theory. *J. Chem. Phys.* **101**, 8964–8971 (1994). doi:[10.1063/1.468447](https://doi.org/10.1063/1.468447)
16. G. Henkelman, H. Jonsson, A dimer method for finding saddle points on high dimensional potential surfaces using only first derivatives. *J. Chem. Phys.* **111**, 7010–7022 (1999). doi:[10.1063/1.480097](https://doi.org/10.1063/1.480097)
17. L. Gámez, B. Gámez, M.J. Caturla et al., Object Kinetic Monte Carlo calculations of irradiated Fe–Cr dilute alloys: the effect of the interaction radius between substitutional Cr and self-interstitial Fe. *Nucl. Instrum. Methods B* **269**, 1684–1688 (2011)
18. C.S. Becquart, C. Domain, An object Kinetic Monte Carlo simulation of the dynamics of helium and point defects in tungsten. *J. Nucl. Mater.* **385**, 223–227 (2009). doi:[10.1016/j.jnucmat.2008.11.027](https://doi.org/10.1016/j.jnucmat.2008.11.027)
19. K. Maier, H. Mehrer, E. Lessmann et al., Self-diffusion in nickel at low temperatures. *Phys. Status Solidi B* **78**, 689–698 (1976). doi:[10.1002/pssb.2220780230](https://doi.org/10.1002/pssb.2220780230)
20. F. Cleri, V. Rosato, Tight-binding potentials for transition metals and alloys. *Phys. Rev. B* **48**, 22–33 (1993). doi:[10.1103/PhysRevB.48.22](https://doi.org/10.1103/PhysRevB.48.22)
21. H.J. Wollenberger, in *Physical Metallurgy*, ed. by R.W. Cahn, P. Haasen (Amsterdam, 1983) pp. 157–158
22. B.W. Zhang, W.Y. Hu, X.L. Shu, in *Theory of Embedded Atom Method and Its Application to Materials Science—Atomic Scale Materials Design Theory* (2003), pp. 84–85
23. J. Bacon, F. Gao, Y.N. Osetaky, Computer simulation of displacement cascades and the defects they generate in metals. *Nucl. Instrum. Methods B* **153**, 87–98 (1999). doi:[10.1016/S0168-583X\(99\)00041-5](https://doi.org/10.1016/S0168-583X(99)00041-5)
24. R.W. Siegl, M.J. Fluss, L.C. Smedskjaer, in *The Application of Position Annihilation in Materials Science* (1982), pp. 1–21
25. A. Seeger, D. Schumacher, W. Schilling, Vacancies and Interstitials in metals, Proceedings of the International conference held at Jülich, Germany, 23–28 Sept 1968 (North Holland publishing company, Amsterdam, 1970), pp. 667–728
26. S.M. Foiles, M.I. Baskes, M.S. Daw, Embedded-atom-method functions for the fcc metals Cu, Ag, Au, Ni, Pd, Pt, and their alloys. *Phys. Rev. B* **33**, 7983–7991 (1986). doi:[10.1103/PhysRevB.33.7983](https://doi.org/10.1103/PhysRevB.33.7983)
27. P Ehrhart, Properties and interactions of atomic defects in metals and alloys, Landolt-Börnstein, New Series III, vol. 25 (1991)